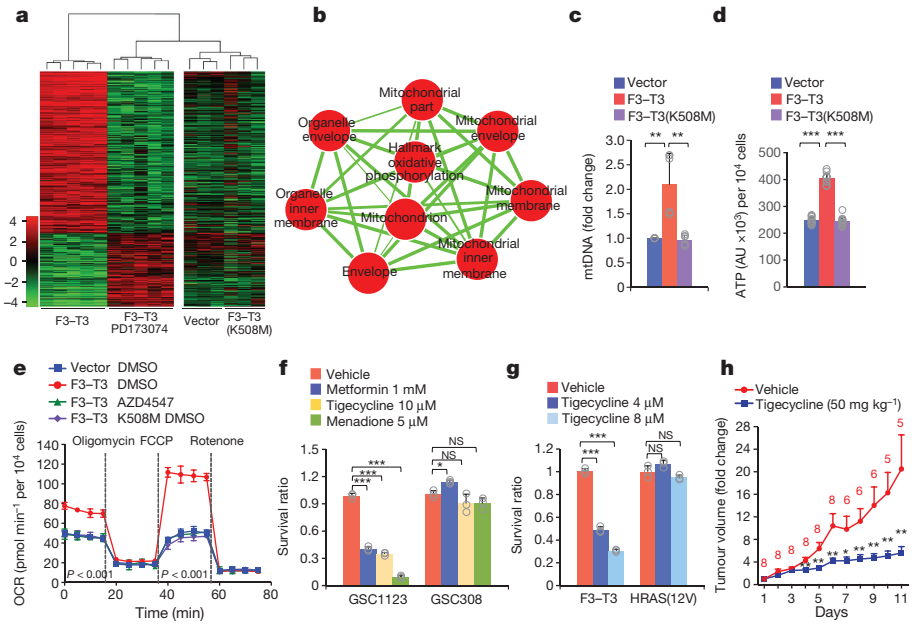

Figure 1 | Activation of mitochondrial biogenesis and metabolism by F3–T3. a, Hierarchical clustering of differentially expressed genes (DEGs) between F3–T3 human astrocytes, F3–T3 human astrocytes treated with PD173074 ($n = 5$ biologically independent samples per group). Human astrocytes expressing the empty vector and F3–T3(K508M) ($n = 3$ biologically independent samples per group) are included as controls. *t*-test $P < 0.01$ and MWW test $P < 0.01$. **b**, Enrichment map network of statistically significant GO categories ($Q < 10^{-6}$ in F3–T3 human astrocytes versus F3–T3 human astrocytes treated with PD173074 and human astrocytes expressing F3–T3(K508M) or vector). Nodes represent GO terms and lines their connectivity. Node size is proportional to the significance of enrichment and line thickness indicates the fraction of genes shared between groups. **c**, qPCR of mitochondrial DNA (mtDNA) in human astrocytes expressing F3–T3, F3–T3(K508M) or vector. **d**, Quantification of cellular ATP in human astrocytes as in **c**. **e**, OCR of F3–T3 human astrocytes treated with or without AZD4547. **f**, Survival ratio of GSC1123 and GSC308 cells following treatment with the indicated mitochondrial inhibitors. **g**, Survival ratio of F3–T3;shTrp53 and HRAS(12V);shTrp53 mGSCs treated with vehicle or tigecycline. **h**, Tumour volume in mice treated with vehicle ($n = 8$) or tigecycline ($n = 10$). Data are fold change ± s.e.m. of controls. The number of mice remaining in the study at each time point is indicated. Data are representative of two (**f**, **g**) or three (**e**) independent experiments. Data are fold change ± s.d. (**c**) or mean ± s.d. (**d**–**g**) of $n = 3$ technical replicates (**e**–**g**) or $n = 6$ (**c**) and $n = 12$ replicates (**d**) from two independent experiments. $^*P \leq 0.05$, $^{**}P \leq 0.01$, $^{***}P \leq 0.001$, two-tailed *t*-test with unequal variance.

volume after six days, the last day on which all controls were alive. At the end of the experiment (day 11), three of the eight mice in the control group had been euthanized, whereas all mice receiving tigecycline were alive ($n = 10$; Fig. 1h and Extended Data Fig. 2n).

To identify F3–T3 substrates that drive oxidative metabolism, we performed anti-phosphorylated tyrosine (phospho-tyrosine) immunoprecipitation of tryptic digests of total cellular proteins from human astrocytes expressing F3–T3, F3–T3(K508M) or the empty vector, followed by identification of phosphopeptides by liquid chromatography–tandem mass spectrometry (Supplementary Table 2). As expected, F3–T3 showed the largest changes in phospho-tyrosine; Y647 in FGFR3 and Y684 in TACC3 showed the highest and second highest enrichment in phosphorylation, respectively. After the enrichment seen in F3–T3, the next most enriched phospho-tyrosine was Y122 of PIN4 (hereafter PIN4(Y122)), a poorly studied homologue of the cancer-driver PIN1 peptidyl-prolyl-*trans*-isomerase[9–11] (Supplementary Table 2). This residue (Y122) is conserved in PIN4 across evolution and we found that F3–T3 interacts with endogenous PIN4 (Extended Data Fig. 3a, b). Analysis of anti-phosphotyrosine immunoprecipitations revealed that only cells expressing active F3–T3 contained tyrosine-phosphorylated PIN4, PKM2, DLG3, C1orf50 and GOLGIN84, whereas tyrosine-phosphorylated HGS was also present in FGFR3-expressing cells (Fig. 2a and Extended Data Fig. 3c, d). Treatment of GSC1123 cells with AZD4547 removed constitutive tyrosine phosphorylation of F3–T3, PIN4, PKM2, GOLGIN84 and C1orf50, whereas phospho-ERK, phospho-Stat3 and phospho-AKT were not changed (Extended Data Fig. 3e, f). We confirmed F3–T3-specific tyrosine phosphorylation of exogenous wild-type PIN4, PKM2, GOLGIN84, DLG3 and C1orf50, but phosphorylation of the corresponding un-phosphorylatable tyrosine to alanine or phenylalanine phospho-mutants was greatly reduced (Extended Data Fig. 3g). We generated and validated a phosphorylation-specific antibody against phosphorylated PIN4(Y122) (phospho-PIN4(Y122)). The antibody detected PIN4 in cells expressing F3–T3, but not in cells transduced with vector, FGFR3 or F3–T3(K508M) (Extended Data Fig. 3h, i). Phospho-PIN4(Y122) was readily detected in F3–T3;shTrp53 mGSCs and xenografts but was absent in HRAS(12V);shTrp53 mGSCs and corresponding tumours (Extended Data Fig. 4a, b). Immunostaining of phospho-PIN4(Y122) in primary human GBM revealed that tumours with F3–T3 ($n = 14$) expressed much higher levels of phospho-PIN4(Y122) than tumours lacking F3–T3 fusions ($n = 35$, 15 of which expressed EGFR–SEPT14, a different receptor tyrosine kinase gene fusion that signals through phospho-STAT3[12]; Fig. 2b and Extended Data Fig. 4c).

Next, we expressed wild-type and the corresponding phospho-tyrosine mutants of PIN4, PKM2, DLG3, C1orf50 and GOLGIN84 in F3–T3 human astrocytes and measured oxidative metabolism. Expression of wild-type and tyrosine to alanine or phenylalanine mutants of PKM2, DLG3, C1orf50 and GOLGIN84 failed to affect the increased OCR profile of F3–T3 human astrocytes (Extended Data Fig. 4d–g). Conversely, PIN4(Y122F) but not wild-type PIN4 (PIN4(WT)) reverted basal and maximum OCR levels of F3–T3 human astrocytes to the levels of vector-expressing human astrocytes (Fig. 2c and Extended Data Fig. 4h). We observed similar effects in F3–T3 human astrocytes in which endogenous PIN4 had been silenced and replaced by the un-phosphorylatable PIN4(Y122F) phospho-mutant (Fig. 2d and Extended Data Fig. 4i). Expression of PIN4(Y122F) and PIN4(Y122A) phospho-mutants reversed the F3–T3-mediated increase in ATP (Extended Data Fig. 4j). Expression of PIN4(Y122F) also impaired soft agar clonogenicity (Fig. 2e).

To identify the gene expression signature associated with F3–T3 in human tumours, we benchmarked different statistical methods for the analysis of imbalanced datasets using synthetic data and the